

Diffusivity and short-time dynamics in two models of silica

Erik Lascaris, Mahin Hemmati, Sergey V. Buldyrev, H. Eugene Stanley, and C. Austen Angell

Citation: *The Journal of Chemical Physics* **142**, 104506 (2015); doi: 10.1063/1.4913747

View online: <http://dx.doi.org/10.1063/1.4913747>

View Table of Contents: <http://scitation.aip.org/content/aip/journal/jcp/142/10?ver=pdfcov>

Published by the [AIP Publishing](#)

Articles you may be interested in

[Search for a liquid-liquid critical point in models of silica](#)

J. Chem. Phys. **140**, 224502 (2014); 10.1063/1.4879057

[Two-state thermodynamics of the ST2 model for supercooled water](#)

J. Chem. Phys. **140**, 104502 (2014); 10.1063/1.4867287

[Low temperature phase properties of water confined in mesoporous silica MCM-41: Thermodynamic and neutron scattering study](#)

J. Chem. Phys. **138**, 204714 (2013); 10.1063/1.4807593

[Dynamic transitions in a two dimensional associating lattice gas model](#)

J. Chem. Phys. **130**, 184902 (2009); 10.1063/1.3129842

[Colloidal dispersions of octadecyl grafted silica spheres in toluene: A global analysis of small angle neutron scattering contrast variation and concentration dependence measurements](#)

J. Chem. Phys. **125**, 044715 (2006); 10.1063/1.2220564



Diffusivity and short-time dynamics in two models of silica

Erik Lascaris,¹ Mahin Hemmati,² Sergey V. Buldyrev,³ H. Eugene Stanley,¹
and C. Austen Angell²

¹Center for Polymer Studies and Department of Physics, Boston University, Boston, Massachusetts 02215, USA

²Department of Chemistry and Biochemistry, Arizona State University, Tempe, Arizona 85287, USA

³Department of Physics, Yeshiva University, 500 West 185th Street, New York, New York 10033, USA

(Received 20 December 2014; accepted 16 February 2015; published online 13 March 2015)

We discuss the dynamic behavior of two silica models, the BKS model (by van Beest, Kramer, and van Santen) and the WAC model (by Woodcock, Angell, and Cheeseman). Although BKS is considered the more realistic model for liquid silica, the WAC model has the unique property that it is very close to having a liquid-liquid critical point (LLCP), and this makes it particularly useful in studying the dynamics of models that do have a LLCP. We find that the diffusivity is a good indicator of how close a liquid is to criticality—the Si diffusivity shows a jump of 3–4 orders of magnitude when the pressure is reduced, which may be interpreted as an abrupt (though not first-order) transition from a high-density liquid state to a low-density liquid state. We show that this transition is captured by the Adam-Gibbs relation, which also allows us to estimate the configurational entropy of the system. © 2015 AIP Publishing LLC. [<http://dx.doi.org/10.1063/1.4913747>]

I. INTRODUCTION

Tetrahedral network-forming liquids such as water, liquid silica, liquid silicon, and liquid germanium display a range of anomalies not found in other liquids. One of the most familiar is the density maximum: water becomes less dense when cooled below the temperature of maximum density (TMD) of 4 °C at atmospheric pressure. This anomaly is also found in silicon¹ and silica.² In some of these liquids, e.g., water, silicon, gallium, and germanium, the density anomaly is related to the surprising but well-known fact that the crystal phase has a lower density than the liquid phase. A diffusion anomaly (an increase in pressure leading to an increase in diffusivity) is also found in these liquids.

Studies of simple models^{3–9} have indicated that these anomalies could be explained by the existence of a competition between two liquid structures of different density. In tetrahedral liquids, these two liquid structures are a collapsed high-density liquid (HDL) and an expanded low-density liquid (LDL). In some cases, these liquids are able to phase segregate, resulting in a liquid-liquid coexistence that may terminate in a liquid-liquid critical point (LLCP). A LLCP has been predicted for several of these tetrahedral liquids based on simulations, although as of yet few LLCPs have been experimentally verified. This is mainly because the LLCP occurs in an area of the phase diagram that is experimentally hard to reach, i.e., the low-temperature supercooled region. One notable experimental observation of a LLCP in a one-component liquid is that of liquid phosphorous,^{10–12} first predicted by *ab initio* simulations that indicate that the transition is between a polymeric network-forming liquid and a molecular liquid of P₄ molecules.¹³

The existence of a LLCP in water has been heavily debated. Some models do not confirm its existence,^{14,15} but others do.^{16–27} Although a LLCP in silica was predicted^{28–31} based on simulations using the BKS (van Beest, Kramer, and van Santen)

silica model³² and the WAC (Woodcock, Angell, and Cheeseman) silica model,³³ recent simulations reaching temperatures lower than previously possible have indicated that this is most likely not the case.³⁴ The BKS model is far from having a LLCP, but the WAC model does come close. The fact that the WAC model lies so close to the threshold of having a LLCP makes it an interesting model for studying the phenomenon of LLCPs in one-component liquids. In our previous paper,³⁴ we focused on the thermodynamical aspects of silica, and in this paper we will investigate the dynamical aspects.

II. METHODS

We run simulations of two different silica models: the BKS model of van Beest *et al.*,³² and the WAC model of Woodcock *et al.*^{33,35} In both models, the SiO₂ liquid is represented by a 1:2 mixture of Si ions and O ions, without any explicit bonds. For the details of both models and our implementation, see Appendix A of Ref. 34.

We use Gromacs 4.6.1,³⁶ with the Ewald sum (PME) for electrostatics. In all cases we use the v-rescale thermostat³⁷ to keep the temperature constant. Many of our runs are done in the constant-volume/constant-temperature (*NVT*) ensemble, but for those in the constant-pressure (*NPT*) ensemble we use an additional Parrinello-Rahman barostat.³⁸ Diffusivities are calculated with Gromacs' `g_msd` utility. All results are obtained with $N = 1500$ ions, unless specified otherwise. The typical time step is 1 fs, but at very low T we increase this to 4 fs and carefully check that these results match those of the 1 fs time step.

We use the root mean square displacement of the oxygen ions to estimate the equilibration time; we define τ as the time at which $\sqrt{\langle r_O(t)^2 \rangle} = 0.56$ nm, i.e., the average time required by an O ion to move twice its diameter of 0.28 nm. We measure τ at each state point (T, P) and verify that each simulation runs

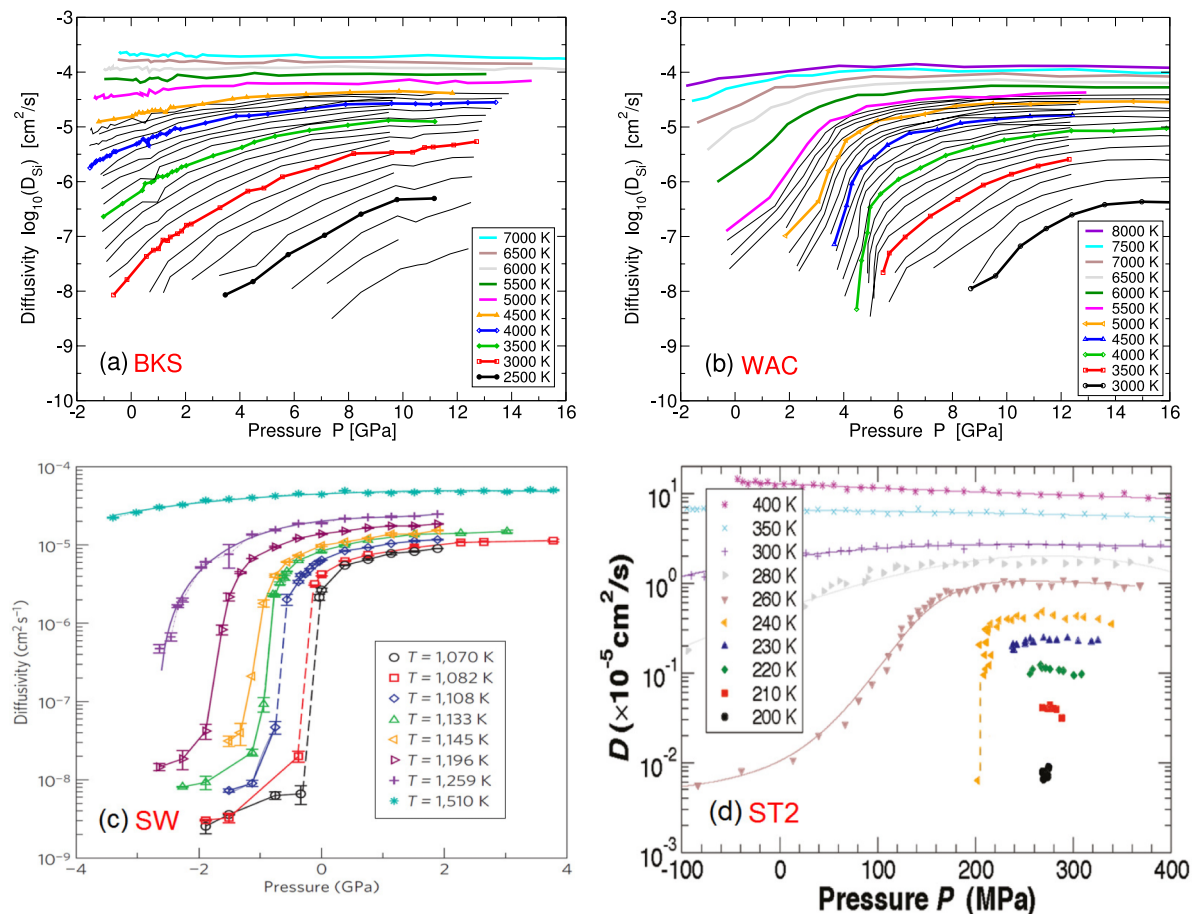


FIG. 1. Diffusivity of the Si atom vs. pressure for several temperatures, in (a) BKS silica and (b) WAC silica. For comparison, panel (c) shows the Si diffusivity in the Stillinger-Weber (SW) model for silicon which is known to have a LLCP at $P = -0.60$ GPa, $T \approx 1120$ K⁴¹ and panel (d) shows the diffusivity for ST2 water,¹⁸ which also has a LLCP. All four panels display a diffusion anomaly, i.e., the diffusivity *increases* with increasing pressure. This increase is gradual for the BKS model (panel (a)), but abrupt in the case of the WAC model (panel (b)) which shows a jump in diffusivity of 3–4 orders of magnitude. The same jump is visible in SW silicon (panel (c)) and ST2 (panel (d)), but here the jump is discontinuous because of the LLCP. In all four models, the low-density liquid state has a much lower diffusivity (and is therefore more “glassy”) than the high-density liquid state, which explains the jump in SW, ST2, and WAC.

for approximately 10τ , well beyond the time necessary for the system to reach equilibrium.

III. DIFFUSIVITY

In most liquids self-diffusion decreases when pressure is increased, but this is not true in all liquids. When a liquid becomes more diffusive as the pressure is increased, we label it a diffusion anomaly. Figure 1 shows diffusivity as a function of pressure for different temperatures. Figure 1(a) shows the Si diffusivity in the BKS model, and Fig. 1(b) the Si diffusivity in the WAC model. As a comparison, Fig. 1(c) shows the same plot for the Stillinger-Weber (SW) model of silicon,³⁹ and in Fig. 1(d) the diffusivity of H₂O molecules in the ST2 water model.⁴⁰ Note that all four models exhibit a diffusion anomaly because they all show an increase in diffusivity when P is increased.

How much the diffusivity increases with pressure differs in each model, however. In the case of SW silicon [Fig. 1(c)], there is a discontinuous jump for $T < 1133$ K at pressures above -0.60 GPa. This is caused by the existence of a LLCP at $T_c \approx 1120$ K, $P_c \approx -0.60$ GPa, which was demonstrated by Vasisht *et al.*⁴¹ At pressures above P_c , the liquid crosses the liquid-liquid

phase transition (LLPT) line, and this is where the jump occurs. At low P the silicon is in a LDL state, which has a very low diffusivity of around 10^{-8} cm²/s. At high P (as well as at high T), liquid silicon is in a HDL state and is much more diffusive ($D_{Si} \sim 10^{-5}$ cm²/s). The same behavior is also found in ST2 water [Fig. 1(d)], which has a LLCP near 240 K and 200 MPa.¹⁸

Figure 1(b) shows how close WAC is to having a LLCP. The jump in diffusivity is as large as in the Stillinger-Weber silicon model, but the isotherms in WAC remain continuous at all pressures. In addition, we see that BKS shows little sign of criticality, although it does show a smooth transition from a high-density liquid to a lower density state at low temperatures.

The BKS model is a better model than WAC for real (experimental) silica⁴² and, since BKS is further away from criticality than WAC, we may conclude that it is unlikely that there is a LLCP in real silica. This conclusion is also indicated by a thermodynamic analysis.³⁴

The diffusivity of the Si ions in liquid silica indicates how well BKS matches experimental results.⁴² Figure 2 shows an Arrhenius plot of our simulation results, combined with results from experiments on amorphous silica. Amorphous silica is a supercooled liquid that moves so slowly that it effectively behaves as a solid. Molecular dynamics simulations are limited

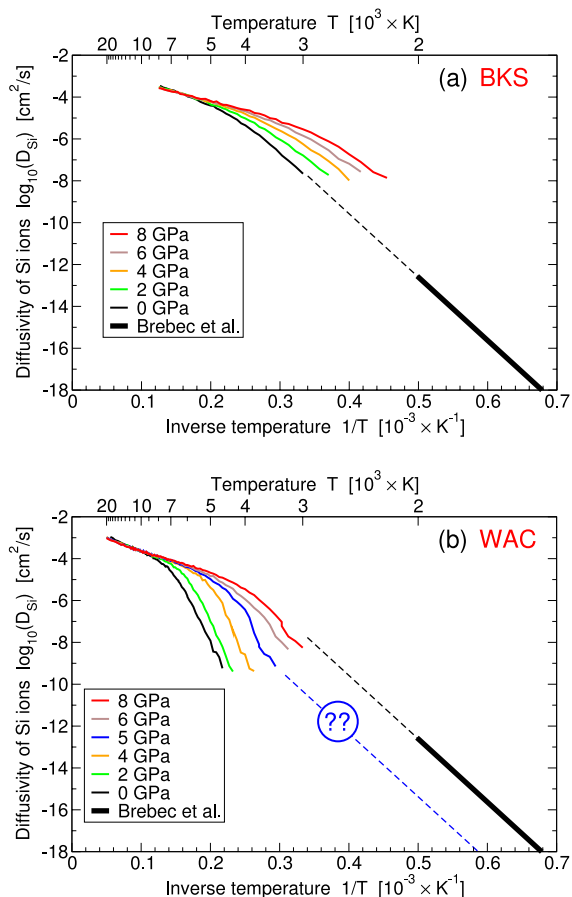


FIG. 2. Arrhenius plot of the Si diffusivity in (a) BKS silica and (b) WAC silica, for several pressures. An extrapolation of experimental results by Brebec *et al.*⁴³ (thick black line) seems to match exactly with the diffusivity of BKS at $P=0$ (dashed black line). On the other hand, the extrapolation does not match with WAC at $P=0$, although it does match approximately at the far higher pressure of 8 GPa. At high T , the liquid is fragile for both models, and shows a transition to a strong liquid upon cooling. The smooth fragile-to-strong transition occurs at roughly the same location as where C_P has its maximum (see Fig. 3). The 5 GPa isobar seems to display an inflection point, after which the curve might continue at a similar slope as the low- T extrapolation in BKS. We shall investigate this hypothesis in more detail at the end of this section.

to runs of several microseconds, and this means the observable diffusivity must be on the order of 10^{-9} cm^2/s and higher. On the other hand, in experiments it is difficult to perform measurements at very short time scales, and the results are therefore limited to diffusivities on the order of 10^{-12} cm^2/s and lower.

Figure 2(a) shows that the diffusivity of BKS simulations at 0 GPa matches the experimental Arrhenius fit $D(T) = (238 \text{ cm}^2/\text{s}) \exp[-(6 \text{ eV})/kT]$ as found by Brebec *et al.*,⁴³ which is a fit that has been experimentally confirmed up to the melting temperature (2007 K) by Wagstaff.^{44–46} A typical explanation for this Arrhenius behavior is that the Si ion needs to overcome a potential barrier E_a to move from one location in the liquid to another, and for a liquid in equilibrium, the probability of acquiring that level of energy is typically $\exp[-E_a/kT]$. Evidently, for BKS at 0 GPa and $T < 4000$ K, the activation energy E_a is about 6 eV, or 579 kJ/mol.

The simulation results of WAC in Fig. 2(b) do not quantitatively match the experimental results, but the qualitative behavior is similar to that of BKS. At high pressures the low- T

slope of WAC is similar to that of BKS ($E_a \approx 6$ eV), but for low pressures the slope of $D(1/T)$ in WAC is much larger, and the activation energy lies around 15 eV (1450 kJ/mol).

Above approximately $D_{\text{Si}} = 10^{-5}$ cm^2/s , the slope of the curves in Fig. 2 is much smaller, and this is known as the “fragile” regime of the liquid (compared to the “strong” regime at low T and $D_{\text{Si}} \ll 10^{-6}$). Thus, upon lowering the temperature, there is a clear fragile-to-strong transition (e.g., around 4000 K for the $P = 0$ curve in BKS). That liquid silica shows a significant deviation from the Arrhenius law at high T has previously been shown in BKS^{47,48} and other models of silica,⁴⁹ and a related deviation has been experimentally witnessed in viscosity data.^{50,51} The strong-to-fragile transition has also been found in simulations of BeF_2 ,⁵² silicon,^{53,54} and water.^{55–57} The origin of this transition is still not fully understood, but it is known⁵⁷ that this transition occurs together with a maximum in the heat capacity C_P (see Fig. 3). Note that the larger and

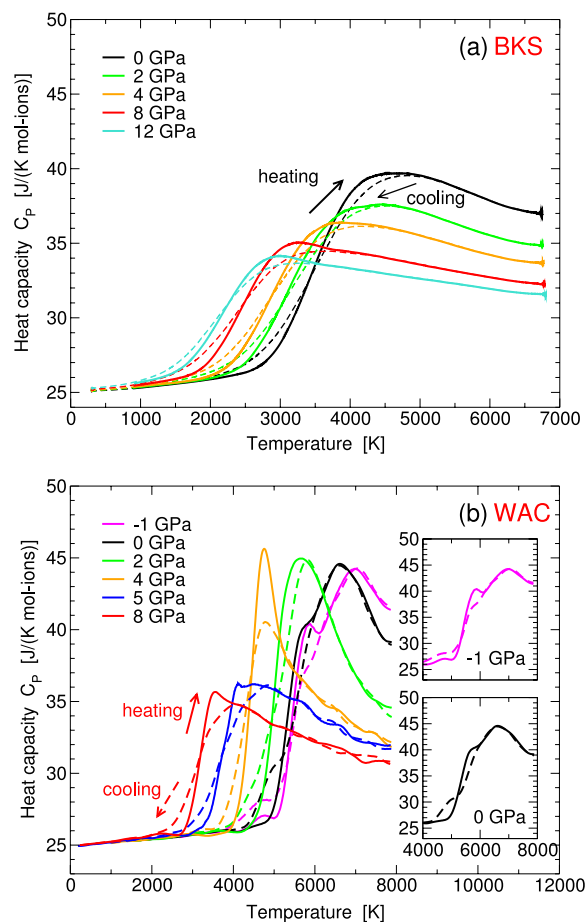


FIG. 3. Heat capacity of (a) BKS and (b) WAC at constant pressure, obtained via repeatedly cooling and heating the liquid at a constant rate (1000 K/ns for BKS, 100 K/ns for WAC). No crystallization occurs during this process; the liquid becomes an amorphous solid at low T instead. The system is no longer ergodic below the temperature where the cooling and heating curves separate, and here the values of C_P are only approximate. Note the occurrence of a second peak in WAC for $P = -1$ GPa, $T \approx 5800$ K observed in the heating part of the cycle (also shown in upper inset), which is caused by the glass transition. At 100 K/ns, the peak is sharp for $P = -1$ GPa, while at $P = 0$ it is reduced to a shoulder (see lower inset). At higher pressures, the ergodic peak disappears as the anomalous domain is exited, and the normal fragile liquid form is recovered. The change in form of heat capacity between ergodic rounded at low pressure and triangular at 10 GPa was also observed in Ref. 31 and used to affirm the onset of a fragile liquid character.

sharper the C_P maximum, the sharper the fragile-to-strong transition.

Figure 3 shows the heat capacity C_P calculated by performing 10 cooling/heating cycles at a rate of 1000 K/ns (100 K/ns for WAC). At a certain temperature the heating and cooling curves separate, and below this temperature the liquid is no longer ergodic. A lower cooling/heating rate causes this separation to occur at a lower temperature. The heat capacity of BKS [Fig. 3(a)] shows a large drop upon cooling, which resembles the drop in C_P that fragile liquids display (note that at these high temperatures silica is fragile rather than strong). This C_P drop is caused by the glass transition,^{58,59} and can be understood as the “freezing in” of the configurational entropy, which means that at low T only the vibrational part of the entropy changes with temperature, and this produces a C_P of about $3R \approx 25$ J/(K mol).

The glass transition is also present in WAC [Fig. 3(b)], with all curves falling to $C_P \approx 25$ J/(K mol) upon cooling. The 8 GPa curve, for example, has a similar shape as the curves in BKS. However, at pressures below 5 GPa, there is a second phenomenon in WAC: as T is decreased, the heat capacity first climbs to a large maximum and then experiences the glass transition drop. At a rate of 100 K/ns, these events cannot be witnessed separately above 0 GPa; the glass transition drop seems to be part of the C_P maximum, and so far these characteristics are as in Ref. 31. That these are in fact two distinct phenomena is clear however, for the -1 GPa curve. At this pressure two peaks are visible, one near 7000 K (the C_P maximum related to the strong-to-fragile crossover) and another tiny peak near 5800 K in the heating curve (related to the glass transition). Exactly the same phenomenon occurs⁸ also in the Jagla model, which has a stable liquid-liquid critical point.

The configurational entropy S_c strongly influences the diffusivity D and the characteristic relaxation time τ . The Adam-Gibbs relation⁶⁰ states that $\tau \propto \exp[A/TS_c]$, with A a constant independent of temperature. Typically, $D \propto 1/\tau$, but previous work⁶¹ indicates that for the Si ions in silica, $D_{\text{Si}}/T \propto 1/\tau$ is a better approximation. Hence, the Adam-Gibbs relation predicts for silica that

$$\frac{D_{\text{Si}}}{T} = \mu_0 \exp\left[-\frac{A}{TS_c}\right], \quad (1)$$

where μ_0 is another temperature-independent constant. This leaves the question of how to obtain the configurational entropy $S_c(T)$. It is possible to calculate S_c directly from the inherent structure energy e_{IS} using^{61,62}

$$S_c(T) = S_c(T_0) + \int_{T_0}^T \frac{1}{T'} \frac{\partial e_{\text{IS}}}{\partial T'} dT' \quad (2)$$

with T_0 as an arbitrary reference temperature. This equation is valid under the assumption that the vibrational free energy does not change substantially from one inherent structure to another, which has been shown to be the case for BKS.⁶¹ The calculation of $e_{\text{IS}}(T)$ is straightforward: we take a configuration of the equilibrated liquid and then minimize the energy using a method such as the conjugate gradient minimization (e.g., the “cg” integrator of Gromacs). We follow this procedure using approximately 2000 configurations for each state point, and

take the average minimized energy as the inherent structure energy e_{IS} .

The calculation of $S_c(T_0)$ is cumbersome, because it requires the calculation of the total liquid entropy $S(T)$ and the vibrational part of the entropy $S_{\text{vib}}(T)$. One way the total entropy can be obtained is via thermodynamic integration of a dilute binary LJ system, combined with the analytical expression of an ideal gas composed of two species of particles. The $S_{\text{vib}}(T)$ can be found using a harmonic approximation of the inherent structures plus an anharmonic correction.⁶¹

We can significantly reduce the effort required to obtain $S_c(T_0)$ if we replace it with a fitting parameter. The Adam-Gibbs relation can then be written as

$$\ln\left(\frac{D_{\text{Si}}}{T}\right) = \ln \mu_0 - \frac{A}{T} \left(S_0 + \int_{T_0}^T \frac{1}{T'} \frac{\partial e_{\text{IS}}}{\partial T'} dT' \right)^{-1}, \quad (3)$$

where μ_0, A, S_0 are fitting parameters and $S_0 \equiv S_c(T_0)$. Using this relation between D_{Si} and e_{IS} , we obtain a reasonable agreement with Ref. 61 for BKS, as shown in Fig. 4. Our calculation of $S_c(T)$ matches that of Ref. 61 when $S_0 \approx 3.64$ J/mol K [see Fig. 4(a)]. In addition, if we set $S_0 = 3.64$ and fit $D_{\text{Si}}(T)$ and $e_{\text{IS}}(T)$ to Eq. (3) using only μ_0 and A as the fitting parameters, we find $\mu_0 \approx 1.64 \times 10^{-7}$ cm²/s K and $A \approx 100$ kJ/mol, and both agree with the results shown in Fig. 15 of Ref. 61.

If we treat S_0 as a fitting parameter, we find similar values for the parameters: $\mu_0 \approx 2.87 \times 10^{-7}$ cm²/s K, $A \approx 147$ kJ/mol, and $S_0 \approx 5.13$ J/mol K, which are all comparable in value to those presented in Ref. 61. The differences occur in part because we do not know the exact relationship between τ and D (which we assumed to be $1/\tau \propto D/T$). In addition, we have imperfect data, i.e., small errors in D and e_{IS} lead to small errors in μ_0, A , and S_0 . Figure 4(b) shows, however, that both

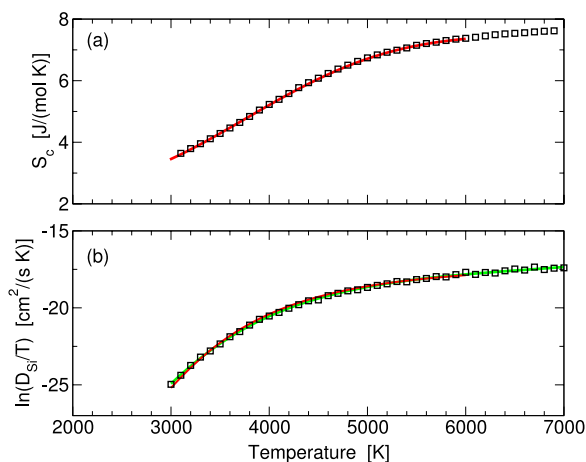


FIG. 4. Fitting the diffusivity D_{Si} to the Adam-Gibbs equation without explicitly calculating the total configurational entropy, for BKS at 2.30 g/cm³. (a) After calculating the average inherent structure energies $e_{\text{IS}}(T)$, we use Eq. (2) to calculate the configurational entropy $S_c(T)$, up to an unknown constant $S_0 \equiv S_c(T_0)$. Comparing our results (black squares) with those of Ref. 61 (red curve), we obtain an estimate of $S_0 \approx 3.64$ J/(mol K). (b) Fitting our D_{Si} data (black squares) using Eq. (3) results in a best fit (green curve) with $S_0 \approx 5.13$ J/(mol K), not too far from the estimated value of 3.64. As a comparison, the fit based on parameters of Ref. 61 are shown as the red curve. Considering that both methods produce similar estimates for S_0 and good fits for $D(T)$, we conclude that treating $S_c(T_0)$ as a fitting parameter (rather than calculating it explicitly) can be done with reasonable accuracy.

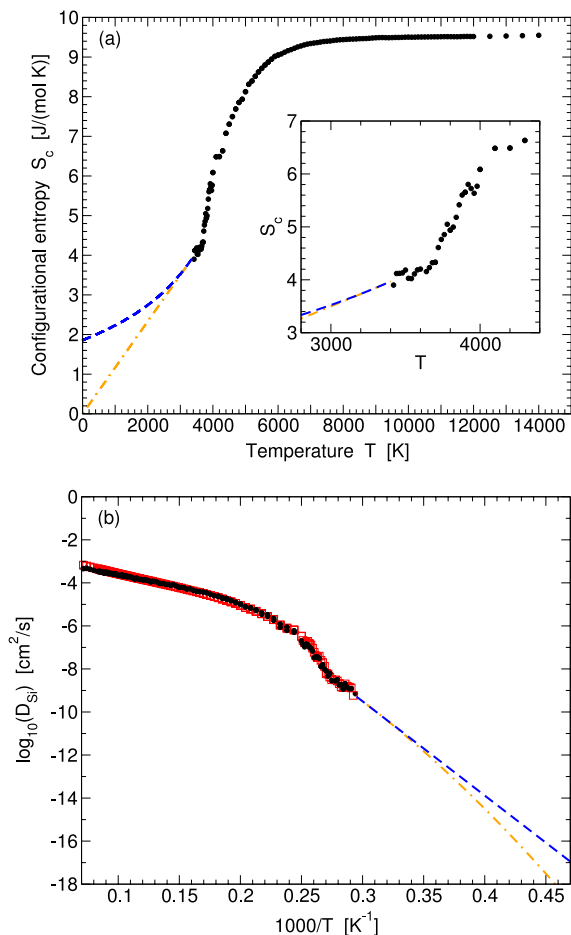


FIG. 5. In WAC at 5 GPa and low temperatures, a kink is visible in both the configurational entropy (panel (a)) as well as in the Si diffusivity (panel (b)). In both panels the black dots indicate data from the simulations, while the red squares in panel (b) are obtained via the Adam-Gibbs relation. Since the black dots and red squares overlap, we find that the kink is also described by the Adam-Gibbs relation. Below 3700 K the configurational entropy changes slope abruptly, and it is unclear what happens in the low- T limit. If we assume the Si diffusivity to be Arrhenius, then the entropy must smoothly saturate to a constant nonzero value (blue dashed curves). However, it is also possible to have a non-degenerate ground state; we find our data to be consistent with a linear decrease in configurational entropy that goes through zero at $T = 0$ (orange dotted-dashed curves).

our parameters and those of Ref. 61 lead to an excellent fit of D vs. T .

Figure 2 indicates that for WAC there might be an inflection point in the $D_{\text{Si}}(1/T)$ of 5 GPa, around 4000 K. We investigate this possibility further in Fig. 5, where we show the configurational entropy calculated via the inherent structure energy, with $S_0 = 3.9$ J/(mol K). This value for S_0 is found by fitting the D_{Si} obtained from simulations [black dots in Fig. 5(b)] to the calculated D_{Si} obtained from Eq. (2) and the inherent structure energies [red squares in Fig. 5(b)]. In addition to $S_0 = 3.9$ J/(mol K), our best fit gives $\mu_0 = 1.165 \times 10^{-3}$ cm²/s and $A = 81.21$ kJ/mol.

Figure 5(a) shows a clear kink in the configurational entropy at approximately 3700 K. This kink provides a convenient escape from the Kauzmann paradox: without the kink, the configurational entropy would extrapolate to zero at some finite temperature T_K , below which the entropy would attain a non-physical negative value. That the kink in $S_c(T)$ happens

around 3700 K is no coincidence, since near this temperature the Si coordination number becomes exactly 4. This indicates that the number of “defects” has been reduced to zero, such that below this temperature all Si ions are bonded with exactly four Si neighbors.⁶³ At finite temperatures, the configurational entropy remains nonzero however, because the Si ions in the liquid can still form rings of different shapes and sizes that all consist of 4-bonded Si ions. As the temperature is lowered further, the ring statistics are reduced to a smaller and smaller set of microstates, which leads to a reduction of the configurational entropy S_c .

Nevertheless, it is unclear how much S_c is reduced as we approach $T = 0$. If we assume that the Adam-Gibbs equation remains valid at low T and that the diffusivity is truly Arrhenius—as seems to be the case for experimental silica—then the configurational entropy needs to smoothly saturate to a constant nonzero value [blue dashed curve in Fig. 5(a)]. However, it is also possible that WAC has a non-degenerate ground state and that $S_c = 0$ at $T = 0$. A physical interpretation of this would be that the glass gradually relaxes upon lowering T until at $T = 0$ it has become a perfect glass.^{64–66} Our data do not refute this scenario. In fact, if we extrapolate the data in Fig. 5(a), we find that $S_c(T)$ drops in a way that is consistent with a linear function that has $S_c = 0$ at $T = 0$, i.e., consistent with the simplest extrapolation [the orange dotted-dashed line in Fig. 5(a)]. Using the Adam-Gibbs equation, we convert this low- T estimate for S_c into a low- T estimate for $D(1/T)$, which is the orange dotted-dashed curve in Fig. 5(b). We see that in this scenario, the behavior of $D(1/T)$ below the kink is not far from an Arrhenius behavior [blue dashed line in Fig. 5(b)].

IV. SHORT-TIME DYNAMICS

Closely related to the diffusivity is the mean square displacement (MSD). In fact, in three dimensions the diffusivity D follows from $\langle |\mathbf{r}(t) - \mathbf{r}_0|^2 \rangle = 6Dt$, in the limit $t \rightarrow \infty$. At very short time scales (on the order of femtoseconds and less) the movement is ballistic, as the atom has not yet felt the forces of its neighbors: $\mathbf{r}(t) \approx \mathbf{r}_0 + \mathbf{v}_0 t$ and thus $\langle |\mathbf{r}(t) - \mathbf{r}_0|^2 \rangle \approx \mathbf{v}_{\text{rms}}^2 t^2$, with $\mathbf{v}_{\text{rms}} = \sqrt{3kT/m}$. At high temperatures the transition from the ballistic regime to the diffusive regime is smooth, but at low temperatures the so-called “cage effect” produces a third regime. In this cage regime the MSD is nearly flat, as the atoms are unable to move past their nearest neighbors for a significant amount of time. Eventually, after a characteristic time known as the α relaxation time, the atoms are able to escape and the MSD increases and becomes diffusive. As the temperature is lowered and the diffusivity decreases, the cage regime spans a longer and longer period of time until the liquid reaches the glass transition and diffusion can no longer be detected. Clearly, the plateau value of the MSD is a good estimate for the cage size.

At low densities, the transition from the ballistic regime to the cage regime is not monotonic, but instead the MSD shows an overshoot around approximately 0.2 ps [Fig. 6(a)]. This overshoot is closely related to the so-called Boson peak in the dynamic structure factor $S(q, t)$, which is the Fourier transform of the MSD. This suggests that the MSD overshoot may be caused by the elasticity of the cage. One can imagine

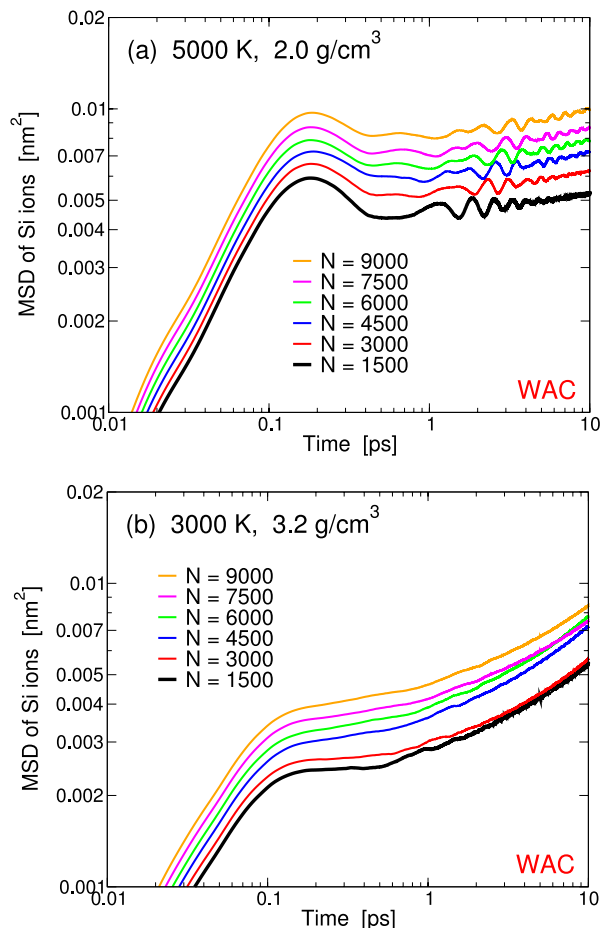


FIG. 6. Mean squared displacement (MSD) of the Si ions in the WAC model, for different system sizes N . Each system consists of $\frac{1}{3}N$ Si ions and $\frac{2}{3}N$ O ions. For clarity, each curve above $N = 1500$ has been shifted by a factor of 1.1 with respect to the curve below it; e.g., $N = 4500$ has been multiplied by 1.1² to prevent overlap with $N = 1500$ and $N = 3000$. In panel (a), the MSD at 5000 K and 2.0 g/cm³ (approx. 1.9 GPa) shows a large MSD overshoot near 0.2 ps, which is independent of the system size. Finite-size effects, however, do lead to the “ringing” effect that can be observed at larger times. The time difference between two consecutive peaks in the ringing regime is approximately given by $\Delta t \approx L/c \approx (0.053 \text{ ps})N^{1/3}$, where L is the size of the box (of total volume L^3) and c the approximate speed of sound.^{67,68} In panel (b), the MSD at 3000 K and 3.2 g/cm³ (approx. 12.4 GPa) is shown, and at these pressures the MSD overshoot and the ringing can no longer be witnessed.

an atom trying to escape its cage by moving in between two of its neighbors, causing these neighbors to move apart slightly. But because these neighbors are also constricted, they cannot open up a space large enough for the atom to move past them. The result is that the atom is bounced back into its cage.

Fig. 6(a) shows that the MSD overshoot is not a finite-size effect, as it is independent of the number of atoms N (to make the individual curves easier to see in Fig. 6, we have shifted each curve up slightly). In addition to the overshoot, there is also a distinct ringing visible at later times, which clearly does depend on the size of the simulation box. At high densities and pressures the MSD overshoot disappears, and with that also the ringing [see Fig. 6(b)]. The ringing is caused by the periodic boundary conditions employed in our simulations, as has also been pointed out by Lewis and Wahnström.^{67,68} Any disturbance that is able to propagate undamped through the

system will leave one side of the box and reenter from the other side. Therefore, each peak in the ringing is a copy of the previous peak that has traveled an additional time of L/c where L is the size of the box and c the approximate speed of the sound wave.

From Fig. 6(a), we estimate that for WAC at 5000 K and 2.0 g/cm³, the time between two consecutive peaks is $\Delta t \approx L/c \approx (0.053 \text{ ps})N^{1/3}$, which corresponds to $c \approx 5 \text{ nm/ps}$. The speed of sound can also be estimated via the adiabatic compressibility, $K_S = 1/\rho c^2$, which can be calculated from the isothermal compressibility and the heat capacities: $K_S = K_T C_V / C_P$. We find these numbers to be in agreement.

Previous studies have argued⁶⁸ that the ringing may disappear when N is made large enough but, as Fig. 6(a) indicates for WAC at low T and low ρ , the ringing remains, even in systems as large as $N = 9000$ ions. A more important factor than the box size is the anharmonicity of the liquid. A liquid that is completely harmonic allows waves to travel through the entire system with little dissipation, while in an anharmonic liquid the frequency of the wave breaks up into many components, which reduces the wave’s amplitude. Thus, the LDL system in Fig. 6(a) is strongly harmonic, which explains why a large box with 9000 ions does not provide sufficient damping. Comparing Figures 6(a) and 6(b), we are therefore able to associate the crossover from strong to fragile liquid thermodynamics of Fig. 3, with a change of harmonic to anharmonic character in the dynamics.

V. DISCUSSION

In Secs. I–IV, we have provided the time-dependent aspects of two distinctly different models of the technically important and academically fascinating substance, SiO₂, for which the equilibrium thermodynamic characteristics were described in an earlier paper.³⁴ The two models have different virtues. For the first model, BKS, our results discussed in Fig. 2(a) provide further evidence that it accurately reproduces the properties of laboratory silica. For the second, WAC, the original SiO₂ simulation model,³³ we have further demonstrated how useful it may be as a model liquid system. While clearly related to the laboratory SiO₂ system, its dramatic variations of dynamic properties with pressure show how closely it approaches actual criticality (and first order polyamorphism). Most interesting in this respect is the clear path that can be seen to the generation of a model ionic system with unambiguous liquid-liquid phase equilibria free from interference by facile crystallization.

Using temperature scanning, the WAC model simulations have revealed that at low pressures there is a clear separation of an anomalous maximum in the equilibrium heat capacity from the kinetic glass transition, something that was formerly only evident in frequency-dependent heat capacity simulations (on the BKS model⁶⁹). In the WAC model, this feature is not only much more prominent, but also sharpens ($\partial^2 C_P / \partial T^2$)_P with increasing pressure, reaching a maximum in sharpness at 4 GPa. The increasing sharpness in heat capacity is correlated with an increasingly sharp deviation from the high temperature diffusivity in the Arrhenius plot, as predicted by the Adam-Gibbs equation.⁶⁰ In principle, this should be accompanied by

a reversion to a low temperature Arrhenius domain such as that calculated, but not yet observed, in the case of supercooled water.⁷⁰ In the case of WAC at 4 GPa, this reversion occurs at too low a diffusivity to be observed within our simulation window, but at the higher pressure of 5 GPa the reversion is seen at the limit of simulation error. The existence of this “fragile-to-strong” liquid transition has been supported by our Adam-Gibbs prediction of the course of the diffusivity at lower temperatures, as was demonstrated in Fig. 5.

In the case of a first order liquid-liquid transition, the decrease in diffusivity is seen as a major discontinuity (which can be attributed to the significant discontinuity in configurational entropy), as seen in Fig. 1 for the two established cases: liquid silicon in the SW model, and ST2 water. The sharp diffusivity plunge in WAC in Fig. 1(b) as pressure changes in the range 2–6 GPa can be regarded as a sort of “critical slowing down” in the vicinity of a critical point. This critical point does not exist in the usual PT -plane but only exists in an additional dimension in parameter space, i.e., we envision that a small change in the parameters of WAC may introduce a LLC.

Thus, we need to determine how to alter the interaction potential of the WAC model in order to change the system to one with an effective critical point and a liquid-liquid coexistence line. In view of the controversies surrounding the subject of polyamorphism, it would clearly be very desirable to have such an example for study. We therefore return briefly to the subject of how to produce the condition for criticality (and then liquid-liquid coexistence), in a SiO_2 -like model.

In our previous paper we suggested that criticality could be engineered by imposing an energy penalty on any Si–O–Si angle that deviates from 180° , in the same way that Stillinger and Weber³⁹ devised their successful potential for liquid silicon. It has been shown previously how the weakening of this tetrahedral bias can also weaken the tendency to crystallize in the SW model and produce a strongly glassforming monatomic liquid.⁷¹ Separately,⁷² using the isochore crossing diagnostic, it has been shown how the glassforming domain in such a modified SW model is reached via a critical point at which the first order transition strength disappears and the glassforming domain begins. An analogous continuous path to criticality can be generated by reversing the above path and going from the present WAC model to a critical model by continuous changes in the tetrahedral reinforcement parameter. A practical motivation for actively pursuing such phenomenology would be the possibility of generating nanoporous amorphous versions of aluminum-free zeolitic structures (currently under study as fuel cell membrane materials).

Unexpectedly, however, we find that there are even simpler ways of inducing criticality in a modified WAC model. In a paper currently in preparation,⁷³ we will describe a modification which produces not only the unambiguous isochore-crossing analogs of Figure 1(b) of our previous paper, but also shows how the progressive perturbation of the WAC potential can result in (i) a systematic shift of the LLC to negative pressures and (ii) the generation of a PT phase diagram that is remarkably similar to that predicted for real water.⁷⁴

Changing the parameters of a model to suppress or enhance a LLC is not a new concept. A study done by Molinero *et al.*⁷¹ shows that reducing the three-body repulsion

parameter λ in the Stillinger-Weber potential³⁹ causes the first order liquid-liquid phase transition in the original model ($\lambda = 21$) to disappear. This parameter is related to the flexibility of the tetrahedral bond angles, and making these more flexible appears to suppress the LLC. The connection between bond angle flexibility and the occurrence of a LLC has also been shown by Tu *et al.* using a different monatomic model,⁷⁵ and more recently by Sciortino and coworkers using models of tetra-functional patchy colloids.^{76–78} The colloidal studies are of particular interest, as it has been shown that with the right choice of parameters it is possible to witness a “crystal clear” liquid-liquid phase transition, as opposed to a transition that occurs between two liquids that are both metastable with respect to the crystal (as has been predicted, e.g., for the case of water for which it had previously been predicted^{3,16,79–81}). Furthermore, it might be possible to construct these colloids in laboratory, thus providing a means to experimentally investigate the phenomenon of liquid-liquid phase transitions in one-component tetrahedral systems.

VI. CONCLUSIONS

Both the analysis of the diffusivity and the analysis of the MSD overshoot indicate a large difference between the low-density region (LDL) of WAC at low T and low P , and the high-density region (HDL). The difference between these two liquid states can be clearly seen in a large number of quantities. LDL is more tetrahedral, has relatively stiff Si–O–Si bond angles, has a more open structure (making it less dense), acts as a strong liquid, and has a MSD that is harmonic. On the other hand, HDL is far less tetrahedral, has flexible bond angles, is a compact liquid, shows fragile behavior, and is anharmonic.

Note that although we can identify two clearly distinct liquid structures in WAC, this does not confirm that WAC displays a liquid-liquid phase transition or has a liquid-liquid critical point. The LDL structure is not sufficiently stable with respect to the HDL at any temperature or pressure and is therefore unable to remain in a (meta) stable equilibrium with HDL. Instead, there is a smooth transition between the two liquid regions, most clearly demonstrated by the smooth jump in diffusivity [Fig. 1(b)]. This change in structure is accompanied by a large but finite C_P maximum [Fig. 3(b)]. The locus of C_P maxima is therefore a good indicator of where the HDL region ends and the LDL region begins, especially since the C_P maximum coincides with the strong-to-fragile transition. The behavior of BKS silica is in many ways similar to that of WAC, but with a smoother LDL-HDL transition.

ACKNOWLEDGMENTS

E.L. and H.E.S. thank the National Science Foundation (NSF) Chemistry Division for support (Grant No. CHE 12-13217). S.V.B. thanks the Dr. Bernard W. Gamson Computational Science Center at Yeshiva College for support. C.A.A. acknowledges the support of this research through the National Science Foundation (NSF) chemistry program under collaborative Grant No. CHE 12-13265.

- ¹M. Watanabe, M. Adachi, T. Morishita, K. Higuchi, H. Kobatake, and H. Fukuyama, *Faraday Discuss.* **136**, 279 (2007).
- ²R. Brückner, *J. Non-Cryst. Solids* **5**, 123 (1971).
- ³P. H. Poole, F. Sciortino, T. Grande, H. E. Stanley, and C. A. Angell, *Phys. Rev. Lett.* **73**, 1632 (1994).
- ⁴E. A. Jagla, *Phys. Rev. E* **63**, 061501 (2001).
- ⁵N. B. Wilding and J. E. Magee, *Phys. Rev. E* **66**, 031509 (2002).
- ⁶P. Kumar, S. V. Buldyrev, F. Sciortino, E. Zaccarelli, and H. E. Stanley, *Phys. Rev. E* **72**, 021501 (2005).
- ⁷L. Xu, S. V. Buldyrev, C. A. Angell, and H. E. Stanley, *Phys. Rev. E* **74**, 031108 (2006).
- ⁸L. Xu, S. V. Buldyrev, N. Giovambattista, C. A. Angell, and H. E. Stanley, *J. Chem. Phys.* **130**, 054505 (2009).
- ⁹K. Stokely, M. G. Mazza, H. E. Stanley, and G. Franzese, *Proc. Natl. Acad. Sci. U. S. A.* **107**, 1301 (2010).
- ¹⁰Y. Katayama, T. Mizutani, W. Utsumi, O. Shimomura, M. Yamakata, and K.-I. Funakoshi, *Nature (London)* **403**, 170 (2000).
- ¹¹Y. Katayama, *J. Non-Cryst. Solids* **312**, 8 (2002).
- ¹²Y. Katayama, Y. Inamura, T. Mizutani, M. Yamakata, W. Utsumi, and O. Shimomura, *Science* **306**, 848 (2004).
- ¹³D. Hohl and R. O. Jones, *Phys. Rev. B* **50**, 17047 (1994).
- ¹⁴L. Xu and V. Molinero, *J. Phys. Chem. B* **115**, 14210 (2011).
- ¹⁵E. B. Moore and V. Molinero, *J. Chem. Phys.* **132**, 244504 (2010).
- ¹⁶P. H. Poole, F. Sciortino, U. Essmann, and H. E. Stanley, *Nature (London)* **360**, 324 (1992).
- ¹⁷P. H. Poole, I. Saika-Voivod, and F. Sciortino, *J. Phys.: Condens. Matter* **17**, L431 (2005).
- ¹⁸P. H. Poole, S. R. Becker, F. Sciortino, and F. W. Starr, *J. Phys. Chem. B* **115**, 14176 (2011).
- ¹⁹F. Sciortino, I. Saika-Voivod, and P. H. Poole, *Phys. Chem. Chem. Phys.* **13**, 19759 (2011).
- ²⁰T. A. Kesselring, G. Franzese, S. V. Buldyrev, H. J. Herrmann, and H. E. Stanley, *Sci. Rep.* **2**, 474 (2012).
- ²¹P. Gallo and F. Sciortino, *Phys. Rev. Lett.* **109**, 177801 (2012).
- ²²Y. Liu, J. C. Palmer, A. Z. Panagiotopoulos, and P. G. Debenedetti, *J. Chem. Phys.* **137**, 214505 (2012).
- ²³P. H. Poole, R. K. Bowles, I. Saika-Voivod, and F. Sciortino, *J. Chem. Phys.* **138**, 034505 (2013).
- ²⁴T. A. Kesselring, E. Lascaris, G. Franzese, S. V. Buldyrev, H. J. Herrmann, and H. E. Stanley, *J. Chem. Phys.* **138**, 244506 (2013).
- ²⁵E. Lascaris, T. A. Kesselring, G. Franzese, S. V. Buldyrev, H. J. Herrmann, and H. E. Stanley, *AIP Conf. Proc.* **1518**, 520–526 (2013).
- ²⁶Y. Li, J. Li, and F. Wang, *Proc. Natl. Acad. Sci. U. S. A.* **110**, 12209 (2013).
- ²⁷J. C. Palmer, F. Martelli, Y. Liu, R. Car, A. Z. Panagiotopoulos, and P. G. Debenedetti, *Nature (London)* **510**, 385 (2014).
- ²⁸P. H. Poole, M. Hemmati, and C. A. Angell, *Phys. Rev. Lett.* **79**, 2281 (1997).
- ²⁹I. Saika-Voivod, F. Sciortino, and P. H. Poole, *Phys. Rev. E* **63**, 011202 (2000).
- ³⁰D. J. Lacks, *Phys. Rev. Lett.* **84**, 4629 (2000).
- ³¹C. A. Angell and M. Hemmati, *AIP Conf. Proc.* **1518**, 9 (2013).
- ³²B. W. H. van Beest, G. J. Kramer, and R. A. van Santen, *Phys. Rev. Lett.* **64**, 1955 (1990).
- ³³L. V. Woodcock, C. A. Angell, and P. Cheeseman, *J. Chem. Phys.* **65**, 1565 (1976).
- ³⁴E. Lascaris, M. Hemmati, S. V. Buldyrev, H. E. Stanley, and C. A. Angell, *J. Chem. Phys.* **140**, 224502 (2014).
- ³⁵M. Hemmati and C. A. Angell, *J. Non-Cryst. Solids* **217**, 236 (1997).
- ³⁶B. Hess, C. Kutzner, D. van der Spoel, and E. Lindahl, *J. Chem. Theory Comput.* **4**, 435 (2008).
- ³⁷G. Bussi, D. Donadio, and M. Parrinello, *J. Chem. Phys.* **126**, 014101 (2007).
- ³⁸M. Parrinello and A. Rahman, *J. Appl. Phys.* **52**, 7182 (1981).
- ³⁹F. H. Stillinger and T. A. Weber, *Phys. Rev. B* **31**, 5262 (1985).
- ⁴⁰F. H. Stillinger and A. Rahman, *J. Chem. Phys.* **60**, 1545 (1974).
- ⁴¹V. V. Vasisht, S. Saw, and S. Sastry, *Nat. Phys.* **7**, 549 (2011).
- ⁴²J. Horbach, W. Kob, and K. Binder, *Philos. Mag. B* **77**, 297 (1998).
- ⁴³G. Brebec, R. Seguin, C. Sella, J. Bevenot, and J. C. Martin, *Acta Metall.* **28**, 327 (1980).
- ⁴⁴F. E. Wagstaff, *J. Am. Ceram. Soc.* **51**, 449 (1968).
- ⁴⁵F. E. Wagstaff, *J. Am. Ceram. Soc.* **52**, 650 (1969).
- ⁴⁶M. L. F. Nascimento and E. D. Zanotto, *Phys. Chem. Glasses: Eur. J. Glass Sci. Technol., Part B* **48**, 201 (2007), available online at <http://www.ingentaconnect.com/content/sgt/ejgst/2007/00000048/00000004/art00001>.
- ⁴⁷K. Vollmayr, W. Kob, and K. Binder, *Phys. Rev. B* **54**, 15808 (1996).
- ⁴⁸J. Horbach and W. Kob, *Phys. Rev. B* **60**, 3169 (1999).
- ⁴⁹M. Hemmati and C. A. Angell, in *Physics Meets Mineralogy: Condensed Matter Physics in the Geosciences*, edited by H. Aoki, Y. Syono, and R. J. Hemley (Cambridge University Press, Cambridge, England, 2000), Chap. 6.1, pp. 325–339.
- ⁵⁰K.-U. Hess, D. B. Dingwell, and E. Rössler, *Chem. Geol.* **128**, 155 (1996).
- ⁵¹E. Rössler, K.-U. Hess, and V. N. Novikov, *J. Non-Cryst. Solids* **223**, 207 (1998).
- ⁵²C. A. Angell, R. D. Bressel, M. Hemmati, E. J. Sare, and J. C. Tucker, *Phys. Chem. Chem. Phys.* **2**, 1559 (2000).
- ⁵³S. Sastry and C. A. Angell, *Nat. Mater.* **2**, 739 (2003).
- ⁵⁴S. S. Ashwin, U. V. Waghmare, and S. Sastry, *Phys. Rev. Lett.* **92**, 175701 (2004).
- ⁵⁵K. Ito, C. T. Moynihan, and C. A. Angell, *Nature (London)* **398**, 492 (1999).
- ⁵⁶P. Gallo and M. Rovere, *J. Chem. Phys.* **137**, 164503 (2012).
- ⁵⁷L. Xu, P. Kumar, S. V. Buldyrev, S.-H. Chen, P. H. Poole, F. Sciortino, and H. E. Stanley, *Proc. Natl. Acad. Sci. U. S. A.* **102**, 16558 (2005).
- ⁵⁸C. A. Angell, *J. Non-Cryst. Solids* **73**, 1 (1985).
- ⁵⁹M. Hemmati, C. T. Moynihan, and C. A. Angell, *J. Chem. Phys.* **115**, 6663 (2001).
- ⁶⁰G. Adam and J. H. Gibbs, *J. Chem. Phys.* **43**, 139 (1965).
- ⁶¹I. Saika-Voivod, F. Sciortino, and P. H. Poole, *Phys. Rev. E* **69**, 041503 (2004).
- ⁶²I. Saika-Voivod, P. H. Poole, and F. Sciortino, *Nature (London)* **412**, 514 (2001).
- ⁶³A. Saksengwijit, J. Reinisch, and A. Heuer, *Phys. Rev. Lett.* **93**, 235701 (2004).
- ⁶⁴C. A. Angell, C. T. Moynihan, and M. Hemmati, *J. Non-Cryst. Solids* **274**, 319 (2000).
- ⁶⁵C. A. Angell, *J. Phys.: Condens. Matter* **12**, 6463 (2000).
- ⁶⁶X. Liu, D. R. Queen, T. H. Metcalf, J. E. Karel, and F. Hellman, *Phys. Rev. Lett.* **113**, 025503 (2014).
- ⁶⁷L. J. Lewis and G. Wahnström, *Phys. Rev. E* **50**, 3865 (1994).
- ⁶⁸J. Horbach, W. Kob, K. Binder, and C. A. Angell, *Phys. Rev. E* **54**, R5897 (1996).
- ⁶⁹P. Scheidler, W. Kob, A. Latz, J. Horbach, and K. Binder, *Phys. Rev. B* **63**, 104204 (2001).
- ⁷⁰F. W. Starr, C. A. Angell, and H. E. Stanley, *Phys. A* **323**, 51 (2003).
- ⁷¹V. Molinero, S. Sastry, and C. A. Angell, *Phys. Rev. Lett.* **97**, 075701 (2006).
- ⁷²V. Kapko and C. A. Angell, “Identifying the zero pressure criticality condition for ‘potential-tuned’ silicon-like liquids by the isochore-crossing diagnostic,” *Chem. Phys. Lett.* (to be published).
- ⁷³E. Lascaris, “Tunable liquid-liquid critical point in an ionic model of silica,” *Phys. Rev. Lett.* (unpublished).
- ⁷⁴R. J. Speedy, *J. Phys. Chem.* **86**, 982 (1982).
- ⁷⁵Y. Tu, S. V. Buldyrev, Z. Liu, H. Fang, and H. E. Stanley, *EPL* **97**, 56005 (2012).
- ⁷⁶I. Saika-Voivod, F. Smallenburg, and F. Sciortino, *J. Chem. Phys.* **139**, 234901 (2013).
- ⁷⁷F. Smallenburg, L. Filion, and F. Sciortino, *Nat. Phys.* **10**, 653 (2014).
- ⁷⁸F. W. Starr and F. Sciortino, *Soft Matter* **10**, 9413 (2014).
- ⁷⁹O. Mishima and H. E. Stanley, *Nature (London)* **396**, 329 (1998).
- ⁸⁰M. Yamada, S. Mossa, H. E. Stanley, and F. Sciortino, *Phys. Rev. Lett.* **88**, 195701 (2002).
- ⁸¹P. G. Debenedetti, *J. Phys.: Condens. Matter* **15**, R1669 (2003).